EXPERIMENTAL EVALUATION OF A MULTIFUNCTIONAL SYSTEM SINGLE-STAGE PV-SHUNT ACTIVE FILTER UNDER PARTIAL SHADING CONDITIONS

P. Robson M. Costa[1], Marcus R. de Castro[1], Isaac R. Machado[1], Edilson M. de Sá Jr.[2]
[1]Universidade Federal do Ceará (UFC), Sobral – CE, Brazil
[2]Instituto Federal do Ceará (IFCE), Sobral – CE, Brazil
email: robsoncee@gmail.com, marcusdecastro@yahoo.com.br, isaacmachado@ufc.br, edilson.mineiro@gmail.com

Abstract **– Distributed solar photovoltaic (PV) generation is becoming more popular. Similarly, the number of electronic loads has increased along with the need to improve power quality. The PV-Shunt Active Filter (PV-SAF) is a system capable of injecting the PV power generated in the electrical grid and eliminating harmonics of current and reactive power of the local installation load. In the single-stage topology, the PV array is connected directly to the SAF DC bus, without the need for an intermediate DC-DC converter. In this paper, a three-phase single-stage PV-SAF system is evaluated in partial shading conditions. For this, a Global Maximum Power Point Tracking (GMPPT) technique capable of quickly tracking the point of maximum power even in the presence of several peaks in the *power-voltage* curve of the PV array is proposed. A night-time mode is implemented for the system operation when there is no PV generation. The instantaneous power theory and the adaptive hysteresis band current controller are used to control the SAF currents. The results obtained through an experimental prototype show that the PV-SAF system with the control strategies adopted is capable of simultaneously injecting into the grid the maximum power of the PV system and compensating harmonics and reactive power.**

Keywords **– DC-AC power converters, Distributed power generation, Maximum power point trackers, Photovoltaic systems, Power conditioning, Shunt active filter.**

I. INTRODUCTION

The distributed generation of solar photovoltaic (PV) has several advantages, such as reducing the power grid demand, thus reducing conduction losses in the grid cables, and allowing consumers to participate in the energy market by selling the surplus generated or by means of energy compensation programs. In addition, the energy generated comes from a clean and sustainable source. With lower costs and increased financial incentives, global PV generation capacity has increased significantly. In 2017, there was a growth of one third, reaching 402 GW [1]. On the other hand, it is useful to measure and limit harmonics and reactive power produced by electronic loads, power supplies, motors, etc. The presence of harmonic currents in power systems or in electrical installations is a relevant problem because it can cause excessive heating in cables and equipment, vibrations and loss of torque in motors, stress and heating in capacitors, failure and reduced life of electronic devices and other sensitive loads. The presence of reactive power in the electric grid can cause conductor overloading, overheating and problems in the voltage level.

The PV generation is usually connected to the electric grid via a Voltage Source Converter (VSC). This structure can also be used simultaneously as a Static Synchronous Compensator (STATCOM) for reactive power support [2]. This system was first called PV-STATCOM by [3]. The first standards for small grid-tied PV systems, such as IEEE 1547:2003 [4] and EN 50160 [5], prevented that these systems from providing reactive support. However, the support of reactive power by PV systems is under discussion in several countries [6]. It is also possible to use the VSC structure of a PV system to act as a Shunt Active Filter (SAF), thus forming the so-called PV-SAF. This system, besides compensating for reactive power of the installation load, can also eliminate current harmonics. IEEE Std. 519:1992 sets limits for harmonic distortion in power systems [7].

The PV-SAF system mainly has two topologies, double-stage or single-stage. The first one has a DC-DC converter to perform the maximum power point tracking (MPPT) of the PV module array and a DC-AC converter to connect to the electric grid. In a single-stage topology, only a DC-AC converter is used to perform the MPPT of the PV array and to connect to the grid. Because this configuration involves fewer components, it has better efficiency than double-stage topology [8], [9]. In [10], a double-stage conversion single-phase PV-SAF system implementation is presented.

In order to extract the maximum power from the PV array, some MPPT techniques were proposed [11], [12]. However, when the PV array is under Partial Shading Condition (PSC), the MPPT can be trapped in some local maximum power peak (LMPP), decreasing system efficiency. Global maximum power point tracking (GMPPT) algorithms ensure that the system will operate on global maximum power peak (GMPP) [13]. The strategies already presented in the literature are diverse, varying in complexity, tracking speed, precision and type of application. These techniques can be classified into three categories: techniques based on conventional methods, techniques that use computational intelligence algorithms and techniques that combine conventional methods with computational intelligence algorithms.

Among the techniques based on conventional methods, [14] estimates the position of the local power peaks using the

Manuscript received 04/05/2020; first revision 06/18/2020; accepted for publication 06/26/2020, by recommendation of Editor Demercil de Souza Oliveira Jr.. http://dx.doi.org/10.18618/REP.2020.2.0020

voltage measured in each one of the modules and use the algorithm Perturb & Observe (P&O) to fine-tune the result, the proposal is simple and fast but requires voltage sensors in each module, which increases the installation complexity and financial costs for implementation. In [15], a region between 50% and 90% of the open circuit voltage (V_{OC}) was defined, and this region is the one with the greatest probability of having GMPP tracked. This region is sliced into parts where P&O is applied. In [16] voltage ramps were used in the entire range from 0 to V_{OC}, instead of steps during GMPPT. This reduces voltage ripple and guarantees a faster sweep in the voltage range. The technique proposed by [17] tracks the global maximum continuously through variations applied to a PI power controller, however the tracking is relatively slow and can generate power losses because it is done continuously, not evaluating the real need to search for the entire curve. In [18], fractions of $0.8 \cdot V_{OC}$ were used to estimate the location of possible power peak, as well as the Hill Climbing method to fine-tune the tracking.

In the category of techniques that use algorithms with computational intelligence, the Particle Swarm Optimization (PSO) algorithm does not depend on information from the PV module manufacturer datasheet or the PV array and requires low computational cost. However, it requires a large number of interactions and produces severe voltage fluctuations during tracking [19]. In [20], the Lagrangian Interpolation was used, by employing information from the PV module manufacturer datasheet, to estimate and direct the initial particles of the PSO technique to points close to possible local peaks (LI-PSO). The convergence time is reduced compared to the traditional PSO. In the Accelerated PSO (APSO) algorithm, proposed by [21], the initial particles are no longer generated randomly and are determined by points in the voltage range. The speed factor is also changed to accelerate convergence. Differential Evolutionary PSO (DEPSO) ensures faster convergence with low computational cost. However, it generates a lot of voltage fluctuation [22]. The Adaptive Velocity PSO (AVPSO) technique minimizes the chances of the particles getting trapped at a local peak, in addition to reducing the voltage fluctuations, as the particles have their positions classified at each iteration [23]. Other computational intelligence techniques were also used in GMPPT, such as the Weibull Pareto Sine-Cosine Optimization (WPSCO) technique used by [24], the Gray Wolf Optimization (GWO) used by [25], the Flower Pollination Algorithm (FPA) used by [26] and the Firefly Algorithm (FA) used by [27] and [28].

Some works have proposed hybrid techniques, which use a conventional method combined with a computational intelligence algorithm to accelerate the tracking convergence or use them in different shading conditions. Regardless of the category, the complexity of the GMPPT technique in PSC increases when compared to conventional techniques used in USC. In this sense, the literature has presented proposals for the detection of PSC and USC, so that the most complex part of the GMPPT is used only in the case of PSC. Thus, GMPP tracking is guaranteed using the appropriate techniques for each type of shading condition. As a result, the tracking time is minimal and prevents loss of power [29], [30].

In PV-SAF systems with single-stage topology, only conventional MPPT techniques were employed, and they were only evaluated under Uniform Shading Condition (USC). Incremental Conductance (IC) algorithm was used in [31] and [32], while [33]–[38] used the P&O algorithm. In these works, the PV array was sized for its maximum power point voltage (V_{MPP}) to match the DC bus voltage of the VSC (V_{DC}). Thus, there is no extensive V_{DC} scan to perform the MPPT.

This work proposes a GMPPT technique for the PV-SAF with a single-stage topology that estimates the LMPP location and verifies which one produces more power. Then, a precise and continuous search with the P&O algorithm is performed while detecting changes in the irradiance conditions and has a night-time mode operation.

Several techniques to generate the reference currents of PV-SAF were used, such as the instantaneous power theory (*p-q* Theory) in [38]–[41], the Synchronous Reference Frame Theory (SRF) in [37] and [33], the Lattice Wave Digital Filter (LWDF) in [42], adaptive controls schemes in [31], the Character of Triangle Function (CTF) in [34], the volterra filter-based control algorithm in [32], the modified Decorrelation Normalized Least Mean Aquare (DNLMS) in [36] and [35], Low-Pass Filters (LPFs) in [43], Robust Extended Complex Kalman Filter (RECKF) in [44] and the Leaky Least Logarithmic (LLL) in [45] and [46]. In the proposed PV-SAF, the *p-q* Theory was used, which is well established and capable of generating reference currents for harmonic and reactive power compensation, in addition to injecting the generated PV power with low total harmonic distortion (THD).

To generate the switching commands in PV-SAF systems already proposed, the hysteresis current control technique was used, which, according to [47], has better performance when compared to Linear Control and Deadbeat Control. The proposed PV-SAF uses an adaptive hysteresis band current controller to generate the switching commands for the VSC. This technique reduces the variation of the switching frequency, the THD of the current and the interference between phases [48]–[50]. The main contributions of this work are:

1) For the first time, PV-SAF with single-stage topology is evaluated experimentally in partial shading condition (PSC);
2) Proposal of a GMPPT algorithm;
3) Sizing of the DC bus voltage range of the VSC;
4) Implementation of night-time mode in PV-SAF;
5) Implementation of adaptive hysteresis band current controller in PV-SAF to improve current control.

The proposed system is evaluated experimentally under different loads and shading conditions.

II. PV-SAF SYSTEM STRUCTURE AND CHARACTERISTICS

Figure 1 shows details of the grid-tied PV-SAF system with three-wire single-stage topology. The PV-SAF system structure consists of a PV module array and a VSC connected by a common capacitive DC bus. The VSC is connected to the point of common coupling (PCC) by

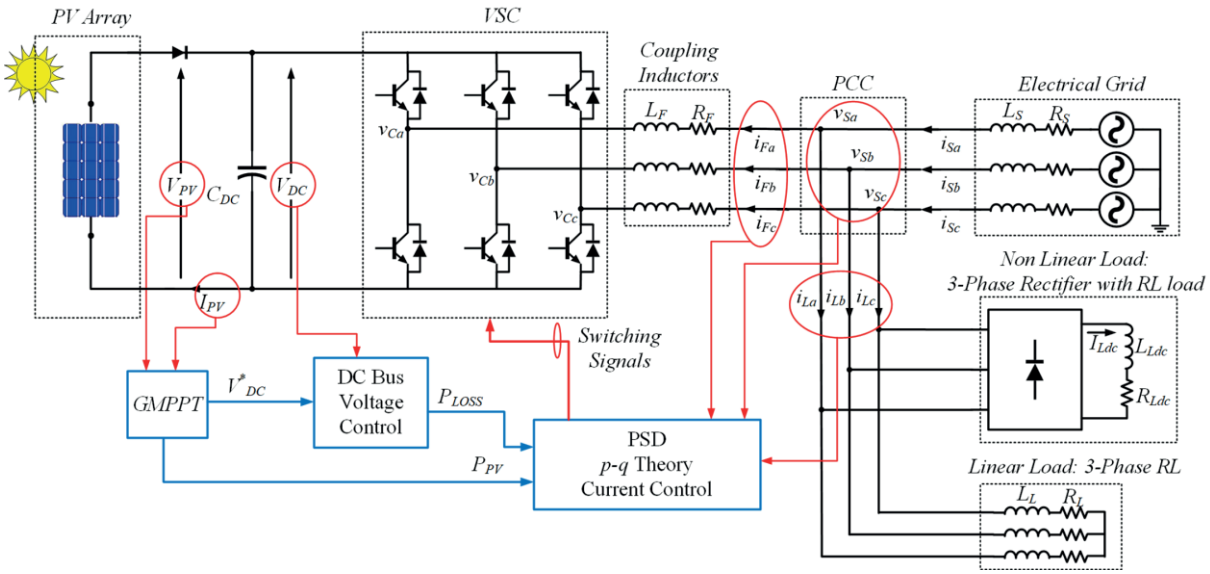

Fig. 1. PV-SAF system configuration and its control schemes.

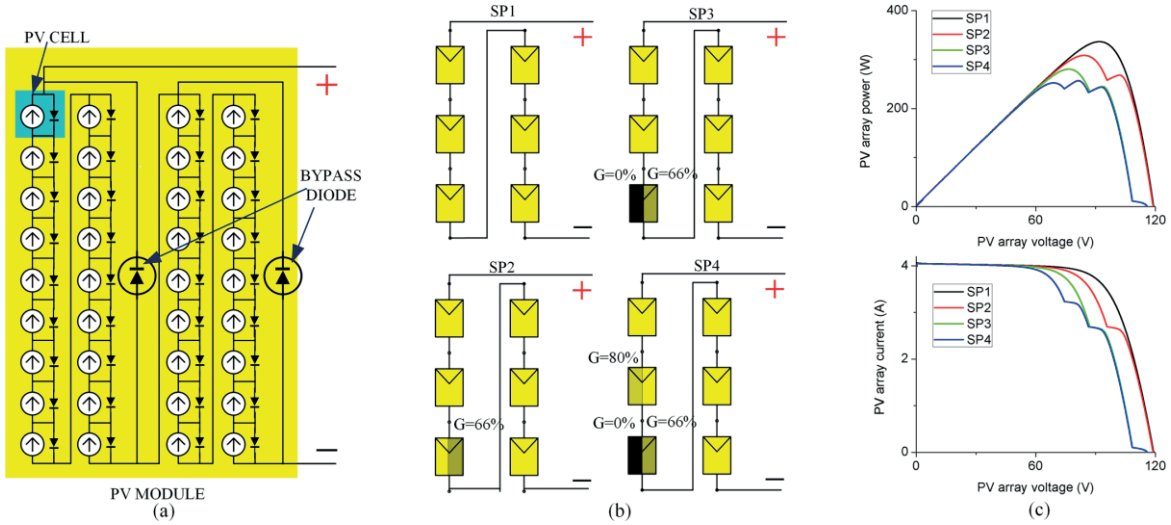

Fig. 2. Kyocera KC65T PV module details (a). PV array under different shading patterns (b) and its *power-voltage* and *current-voltage* curves obtained through PSIM application (c).

coupling inductors that limit the output current ripple. The electric grid and the load, which can be linear or non-linear, also are connected to the PCC. The load currents (i_{Labc}), the PV-SAF currents (i_{Fabc}), the PCC voltages (v_{Sabc}), the DC bus voltage (V_{DC}=V_{PV}) and the PV array current (I_{PV}) are measured. The control systems operate to:

1) Perform the proposed GMPPT and control V_{DC};
2) Obtain the grid voltage positive-sequence component and calculate the reference currents for PV power injection and undesired load current component compensation using the *p-q* Theory;
3) Generate the switching signals using the adaptive hysteresis band current controller.

To propose a GMPPT algorithm, the following section presents the PV array behavior in PSC.

III. PV ARRAY CHARACTERISTICS UNDER PSC

To implement the GMPPT algorithm, it is important to understand how a PV array behaves under PSC. The PV array considered consists of a set of PV modules connected in series to reach the required voltage.

A PV module is composed of a series of PV cells that converts the energy of light directly into electricity by the photovoltaic effect. The PV cell's electric model contains a diode in parallel with a current source, a series resistor (R_S), and a shunt resistor (R_{sh}) [51]. The output current of the PV cell (I_{cell}) is given by

$$I_{cell} = I_{ph} - I_0\left(e^{q(V_{cell}+I_{cell}R_S)/\eta kT} - 1\right) - \frac{V_{cell}+I_{cell}R_S}{R_{sh}} \qquad (1)$$

where k is the Boltzmann constant, q is the elementary charge, η is the diode ideality factor, T is the temperature in Kelvin, I_{ph} is the photocurrent, I_0 is the diode reverse saturation current and V_{cell} is the PV cell output voltage.

Figure 2.a shows how PV cells are placed in the KC65T module manufactured by *Kyocera*. This module has 36 cells and a bypass diode for each string of 18 cells. When a PV cell is shaded, the current of all other cells of the same string is affected. In order not to limit the entire array or module

current by a less-illuminated cell, bypass diodes are used. This diode acts as an alternative path for the current and limits heat dissipation in the shaded cell [51].

Figure 2.b shows an array of 6 KC65T modules connected in series and subject to four different shading patterns (SP1, SP2, SP3 and SP4). The module temperature considered is T=50 °C and the irradiance is G=1000 W/m². The shaded modules are under a fraction of this irradiance, as shown in the figure. As shown in Figure 2.c, the *power-voltage* (*p-v*) curve of the PV array for SP1, obtained through simulation in the PSIM 9.0 simulator, has only one power peak when all modules are subjected to the same irradiance (USC). However, each cell string with a bypass diode can produce a power peak on the *p-v* curve if it is subject to different irradiance from the other cell strings. Thus, in the case of the studied array, since there are 6 modules connected in series and each module has 2 cell strings with bypass diodes, it is possible to produce up to 12 (total bypass diodes) power peaks in the *p-v* curve of the PV array, if each of these cell strings is subject to a different irradiance [52].

IV. PV-SAF CONTROL STRATEGY

The proposed PV-SAF control strategy is divided into three main functions. The first one consists of the GMPPT algorithm for extracting the maximum power available in the PV array. The second is the *p-q* Theory used to generate the reference currents. And, finally, the third is the current control technique.

A. GMPPT Algorithm

The Fractional Open-Circuit Voltage technique has been employed to estimate the GMPP location using $V_{MPP}=N\cdot k_1\cdot V_{OC,m}$, where N is the number of modules connected in series, $V_{OC,m}$ is the module open circuit voltage and k_1 is a proportionality constant and has a value between 0.71 and 0.85 [11], [53]. This technique has an advantage of being easy to be implemented; however, when a PV array is in PSC or when N is large, this relation presents an extremely high estimation error and becomes unusable. To improve this relation, [54] proposes a way to estimate the possible power peak location by (2).

$$V_{MPP,j}=[\alpha\cdot(j-1)+k]\cdot V_{OC,m} \quad (2)$$

In (2), α and k are constants that depend on the module physical characteristics and the operating conditions. $V_{MPP,j}$ is the voltage relative to the *j-th* MPP, where j is the number of the possible power peaks that vary from N to 1. However, as seen in Figure 2, the number of possible power peaks is equal to the bypass diode number in the array and it is possible to occur PSC in one module. Therefore, considering N_{bd} as the bypass diode number in each module, (2) can be rewritten as

$$V_{MPP,j}=[\alpha\cdot(j-1)+k]\cdot(V_{OC,m}/N_{bd}) \quad (3)$$

where j varies from $N_{bd}\cdot N$ to 1. Just like k_1, the value of k can vary from 0.71 to 0.85. According to [54], constant α can take values between 0.8 and 0.97, and it was used as a function of the irradiance on the modules. However, it is difficult to obtain the value of the irradiance in practice. Even using pyranometers or PV reference cells for each module, it is possible that the measurement of these sensors does not reflect reality, since it is common to experience shading only in part of the module. Thus, this work proposes the use of a fixed value for α, like what happens with the constant k. Thus, it is still possible to make a more accurate estimate compared to the Fractional Open-Circuit Voltage technique.

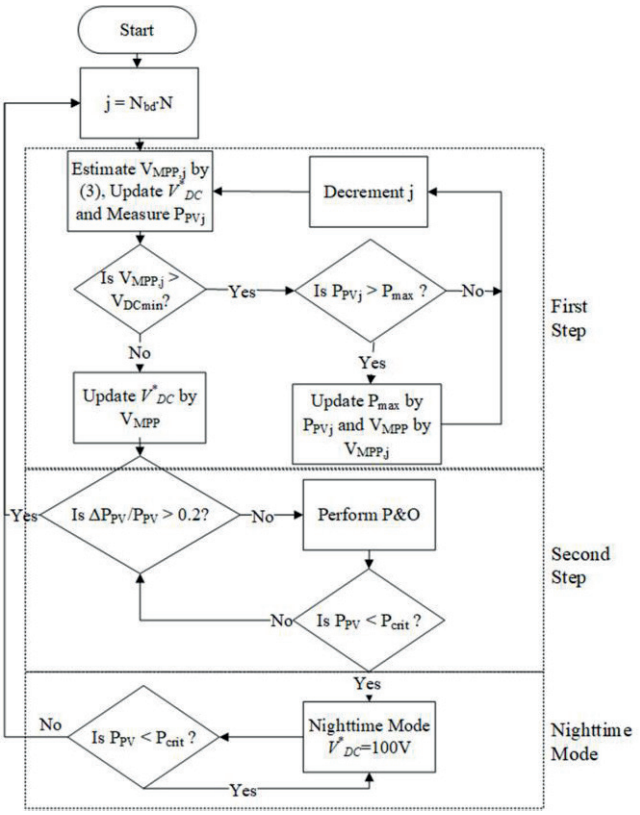

Fig. 3. Proposed GMPPT algorithm flowchart.

The parameters α and k are obtained from the analysis of the *p-v* curves of the PV array under various shading conditions. The values are chosen to obtain the smallest estimation error in several shading patterns. For the case of a PV array formed by the series association of 6 modules Kyocera KC65T, the constants obtained are α=0.9 and k=0.6. The average estimation error was reduced from 4.2 V to 1.3 V compared to the conventional Fractional Open-Circuit Voltage technique.

Figure 3 shows the flowchart of the proposed GMPPT algorithm. Using (3), in addition to considering the possible occurrence of partial shading in a PV module, it is possible to find the GMPP more quickly by jumping directly between points where the LMPPs would appear and measure which of these peaks is the highest.

In the first step, the tracking starts at the rightmost LMPP on the *p-v* curve ($j=N_{bd}\cdot N$). The peak location ($V_{MPP,\ j}$) is estimated by (3). The estimated voltage values are used as a reference for the voltage controller (V^*_{DC}). The PV power generated at each possible peak (P_{PVj}) is measured. The variable j, which represents the current peak, is decremented until the estimated voltage is less than the minimum

allowable voltage to the system (V_{DCmin}). To maintain acceptable controllability in the SAF current, V_{DC} must be within a permissible voltage range. According to [55], the minimum value for V_{DC} (V_{DCmin}) as a function of the grid voltage (V_S) is

$$V_{DC\min} = 2\frac{\sqrt{2}}{\sqrt{3}}V_S, \quad (4)$$

then, $V_{MPP,j}<V_{DCmin}$ is the condition for stopping searching and returning to the peak that led to the highest power.

After that, in the second step, the algorithm executes the P&O function to fine-tune the GMPP. It was set to small voltage steps to avoid voltage ripple.

While performing the P&O function, the proposed GMPPT algorithm verifies if the generated power (P_{PV}) has changed more than 20%. If that is the case, then the GMPPT restarts. During this stage, it is also verified if P_{PV} is smaller than P_{crit} to enter in Night-time Mode. In this mode, the generated power is negligible and the PV-SAF operates with V_{PV} maintained at 100 V for better harmonics compensation. P_{crit} was set at 15 W and $V_{OC,m}$ equal to 19.7 V, relative to the temperature of 47 °C.

The proposed GMPPT algorithm generates the reference voltage for DC bus (V^*_{DC}). This reference is the input for the DC bus voltage scheme control, as shown in Figure 4. The proportional gain and the integrative time obtained for the PI (proportional-integral) voltage controller are 35.2 and 0.00286 s, respectively.

B. SAF Control

Figure 4 shows the PV-SAF scheme control using the *p-q* Theory. To compensate for harmonic current components when the grid voltage is distorted, as can be observed in real environments, the Positive-Sequence Detector (PSD) is used to extract the fundamental positive sequence component of the grid voltage. The electric grid phase angle (θ_S) is obtained by a Quadrature Phase-Locked Loop (QPLL) [56]. The PSD is based on the *p-q* Theory, the auxiliary currents ($i_{1\alpha}$ and $i_{1\beta}$) are used to calculate the auxiliary real power (p_1) by (5). The continuous component of p_1 ($\bar{p}_1$) is extracted by a Low-Pass Filter (LPF) and used to calculate the fundamental positive-sequence grid voltage in α-β axis ($v_{S1\alpha\beta}$) by (6) [39].

$$p_1 = v_{S\alpha}i_{1\alpha} + v_{S\beta}i_{1\beta} \quad (5)$$

$$\begin{bmatrix} v_{S1\alpha} \\ v_{S1\beta} \end{bmatrix} = \frac{1}{{i_{1\alpha}}^2 + {i_{1\beta}}^2}\begin{bmatrix} i_{1\alpha} \\ i_{1\beta} \end{bmatrix}\bar{p}_1 . \quad (6)$$

The reference currents were generated using the *p-q* Theory. The load demands include real power (p_L) and imaginary power (q_L) and are calculated by (7). Generally, the real and imaginary powers have two components: an average one ($\bar{p}_L$ and $\bar{q}_L$) and an oscillating one ($\tilde{p}_L$ and $\tilde{q}_L$).

$$\begin{bmatrix} p_L \\ q_L \end{bmatrix} = \begin{bmatrix} v_{S1\alpha} & v_{S1\beta} \\ v_{S1\beta} & -v_{S1\alpha} \end{bmatrix}\begin{bmatrix} i_{L\alpha} \\ i_{L\beta} \end{bmatrix} = \begin{bmatrix} \bar{p}_L + \tilde{p}_L \\ \bar{q}_L + \tilde{q}_L \end{bmatrix} . \quad (7)$$

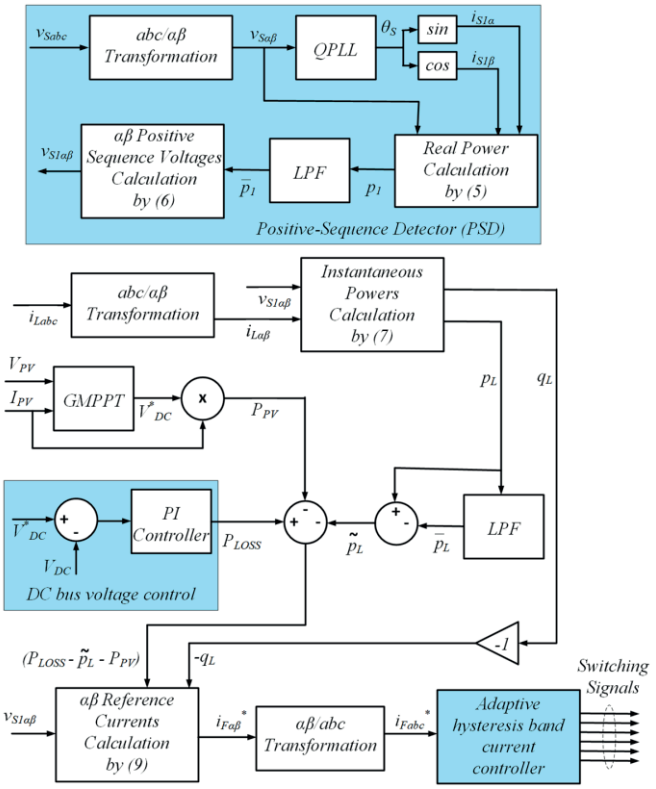

Fig. 4. PV-SAF scheme control using *p-q* theory.

The load power components chosen to be compensated are $\tilde{p}_L$ and q_L, referring to the harmonics and current phase displacement in relation to the PCC voltage, respectively. Thus, the reference powers for the PV-SAF (p^* and q^*) are calculated in (8), where P_{LOSS} is the output of the DC bus voltage controller and equals the converter losses. In (8), the positive power components are drained, and the negative ones are injected by the PV-SAF in PCC.

$$\begin{aligned} p^* &= P_{LOSS} - \tilde{p}_L - P_{PV} \\ q^* &= -q_L . \end{aligned} \quad (8)$$

The reference currents ($i^*_{Fαβ}$) are then calculated by (9) and transformed from α-β axis to *abc* axis (i^*_{Fabc}) to be used by the current controller.

$$\begin{bmatrix} i^*_{F\alpha} \\ i^*_{F\beta} \end{bmatrix} = \frac{1}{{v_{S1\alpha}}^2 + {v_{S1\beta}}^2}\begin{bmatrix} v_{S1\alpha} & v_{S1\beta} \\ v_{S1\beta} & -v_{S1\alpha} \end{bmatrix}\begin{bmatrix} p^* \\ q^* \end{bmatrix} . \quad (9)$$

C. Current Control

To control the converter currents and generate the switching signals, the Hysteresis Current Controller (HCC) is the most used controller in the PV-SAF systems [38], [44], [46]. According to [47], the hysteresis controller shows better performance in Active Filter applications. The main advantages of the HCC are simple implementation, robustness, excellent dynamic performance and independence of load parameters. In addition, this controller tracks the reference current without ripples or delays that may occur in other controllers, such as those that have

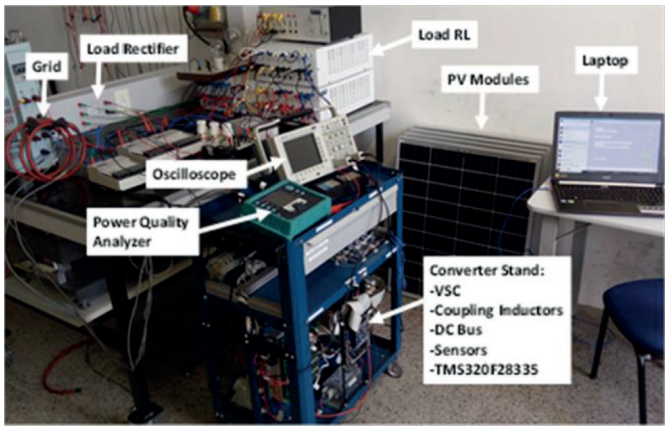

Fig. 5. Photograph of system prototype in the laboratory.

integrators (PI, LQR and LQG controllers). The disadvantages of this controller are limitation by sampling frequency, switching frequency that is variable and dependent on the load time constant, which makes it difficult to design the coupling inductors.

In the proposed PV-SAF system, the Adaptative Hysteresis Band Current Controller (AHBCC) was used. This controller has a dynamic hysteresis band to reduce the switching frequency variation, in addition to minimizing the harmonic distortion rate and reducing interference from phase currents [48]–[50].

Unlike the conventional HCC, which uses the fixed hysteresis band, the AHBCC uses measurements of the DC bus voltage (V_{DC}), the grid voltage (V_{Sabc}) and the derivative of the instantaneous reference current for compensation (di_{Fabc}^{*}/dt) to calculate the hysteresis band and thus reduce the switching frequency variation.

The dynamic Hysteresis Band (HB) of each phase is calculated by (10), and the parameters used are shown in Table I.

$$HB_{abc} = \frac{V_{DC}}{8 f_S L_F}\left[1 - \frac{4L_F^{\,2}}{V_{DC}^{\,2}}\left(\frac{V_{Sabc}}{L_F} + \frac{di_{Fabc}^{\,*}}{dt}\right)^2\right] \quad (10)$$

The DC bus maximum voltage allowed (V_{DCmax}) is calculated to maintain the current ripple within the acceptable magnitude. In this work, it was calculated according to [57], and the value is shown in the Table I.

In a simulation of practical application at a voltage of 380 V, PV array of 30 modules and a 17 kVA converter, the allowable DC voltage would be in the range of 620 V to 840 V.

V. EXPERIMENTAL EVALUATION OF PV-SAF SYSTEM

To validate the proposed control system and strategies, a prototype of the PV-SAF system was implemented in the laboratory and subject to tests. Table I presents the electrical grid and SAF parameters used. A photograph of the system prototype developed in the laboratory is depicted in Figure 5. The converter stand used is equipped with a VSC, current and voltage sensors, coupling inductors, DC bus and with a DSP TMS320F28335 for digital processing of the control.

TABLE I
Grid and SAF Parameters

Symbol	Parameter	Value
V_S	Electrical grid line voltage	40 V
f	Electrical grid fundamental frequency	60 Hz
R_S	Electrical grid series resistor	0.5 Ω
L_S	Electrical grid series inductance	0.6 mH
R_F	Coupling resistance	0.5 Ω
L_F	Coupling inductance	2 mH
C_{DC}	DC bus capacitance	1100 µF
V_{DCmin}	DC bus minimum voltage	65.3 V
V_{DCmax}	DC bus maximum voltage	236 V
$S_{PV\text{-}SAF}$	Converter Power	2.08 kVA
f_S	Sampling frequency	48 kHz

TABLE II
PV Parameters Under Standard Test Conditions (STC*)

Parameter	Value
Cell number	36
Maximum Power	65 W
Maximum Power Voltage	17.4 V
Maximum Power Current	3.75 A
Open Circuit Voltage	21.7 V
Short Circuit Current	3.99 A

*STC: Irradiance 1000 W/m², AM1.5 spectrum, module temperature 25 °C

A series array of 6 PV modules KC65T from the manufacturer *Kyocera* was used. The electrical parameters of this module model are specified in Table II.

In the following subsections several tests under different conditions of shading, irradiation and different types of loads are presented to prove the multifunctional characteristic of the proposed system, as well as the operation and the advantages of the control strategies adopted.

A. Injecting PV power into the grid under different shading conditions and non-linear load

The performance of the proposed GMPPT technique is analyzed under different shading conditions. Simultaneously, the SAF acts to compensate harmonics and reactive power of a non-linear load composed of a three-phase rectifier bridge with *R-L* load (R=26 Ω and L=80 mH). The active power of this load at the fundamental frequency is 113 W. Some materials were applied to cover a set of cells in the PV module to allow the incidence of irradiance (G) in three levels (0%, 66%, and 80%) to simulate a partial shading condition. The *p-v* curves in Figure 6, obtained experimentally for four shading patterns (SP1, SP2, SP3, and SP4), match the curves obtained from the PSIM simulation in Figure 2.c. Of course, there may be some difference in magnitudes due to variations in solar irradiance and temperature during the capture of results. Since each module has 2 bypass diodes, each cover material was placed to cover only cells that are in the string of the same bypass diode, as shown in Figure 2.

The experimental result of the proposed GMPPT performance in the PV-SAF system under different shading conditions and non-linear load is shown in Figure 7. It may be noted that the voltage variation on the DC bus during tracking can modify the shape of the grid current, but only

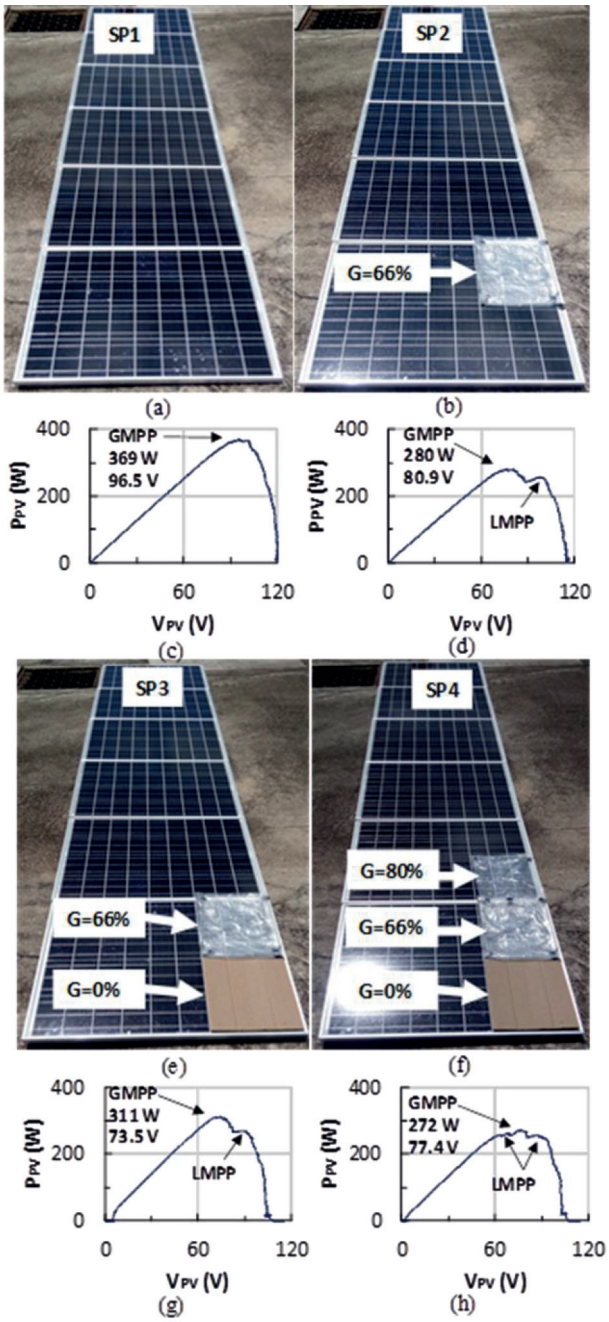

Fig. 6. Experimental PV array characteristics under different partial shading conditions. Shading patterns SP1 (a), SP2 (b), SP3 (e) and SP4 (f) and their respective *p*-v curves (c), (d), (g) and (h).

during the short GMPPT execution time. Note that after the GMPPT execution, the electrical grid current is now sine-shaped due to the correct action of the harmonic compensation by the SAF.

It can also be verified that the GMPP found matches to the GMPP of Figure 6 obtained previously, which proves the good performance of the proposed GMPPT technique even in PSC. Small differences are noted due to irradiance and temperature variations during the tests. The time to reach the GMPP in these conditions averaged 45 ms. In all shading patterns, the PV array generates more power than the load demand. Consequently, the excess power is injected into the electric grid. It can also be observed that the open circuit voltage in the shading patterns SP3 and SP4 is reduced since

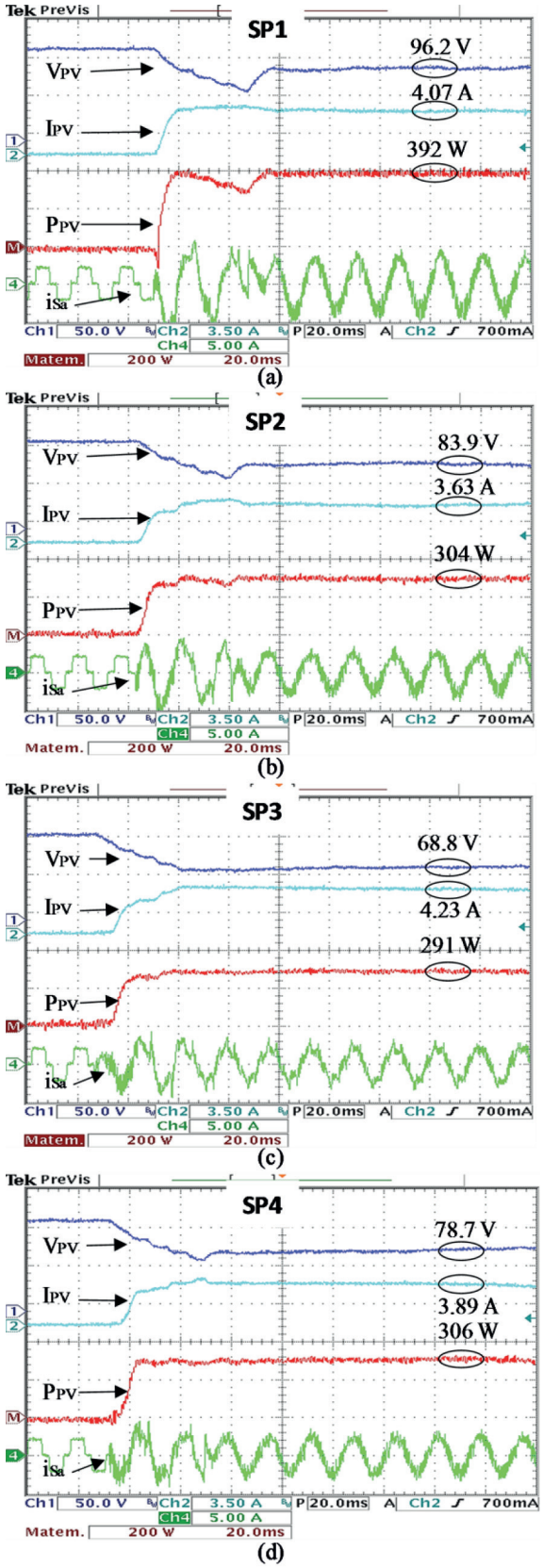

Fig. 7. Performance of injecting PV power into the grid under non-linear load and shading pattern SP1 (a), SP2 (b), SP3 (c) and SP4 (d).

the 6 completely shaded cells (G=0 W/m²) limit the generation of all 18 cells in series that are paralleled with a bypass diode. The generated power is higher under USC (SP1).

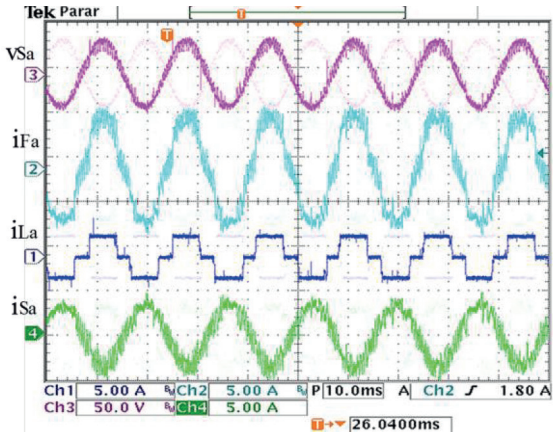

Fig. 8. Performance of PV-SAF with a non-linear load (113 W) lower than PV power generation (370 W).

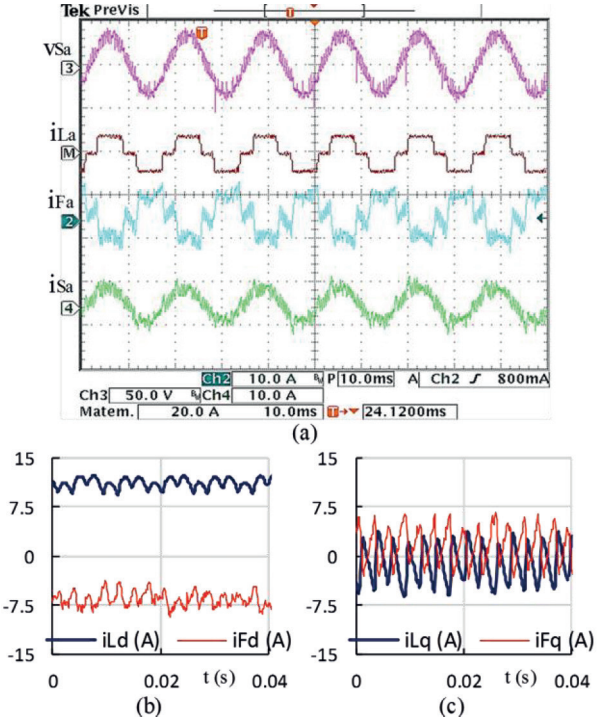

Fig. 9. Performance of PV-SAF with a non-linear load (422 W) greater than PV power generation (330 W) (a). The *d*-axis (b) and *q*-axis (c) load and VSC currents.

To obtain less distortion in the injected current, parameters on the GMPPT algorithm can be set to get a longer tracking time. In real systems in distribution voltage, the tracking time can be longer due to the bigger DC bus capacitance, bigger PV array and bigger DC voltage range allowed. Considering a system at a grid voltage of 380 V and a PV array of 30 modules, through simulations, the GMPPT tracking time averaged 144 ms.

In [31] and [33], for example, in which IC and P&O algorithms were used as MPPT in single-stage PV-SAF systems and did not consider the occurrence of PSC, the reduction of power generated would be 12.9% and 13.5% in the shading patterns SP3 and SP4, respectively. Depending on the shading condition, virtually all generation could be compromised without the performance of a GMPPT. Thus, the strategy proposed becomes more advantageous, extracting the maximum possible power provided by the PV

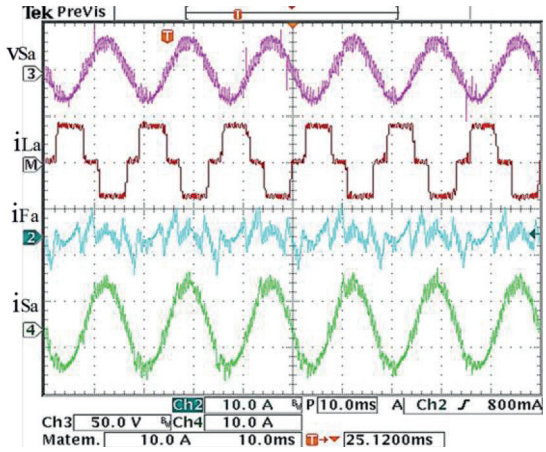

Fig. 10. Performance of PV-SAF at Night-time Mode with a non-linear load (422 W) and V_{DC}=100 V.

array even in PSC within the allowable voltage range for V_{DC}.

B. Performance of PV-SAF Under Non-Linear Load During PV Power Generating

Now, the performance of PV-SAF under different loads is analyzed, keeping the PV generation at USC (SP1). Figure 8 shows the performance of PV-SAF under non-linear load with demand lower than the PV power generated. The load is a three-phase rectifier bridge with load *R-L* (R=26 Ω and L=80 mH) that demands 113 W, and the PV Array generates 370 W. The excess power generated is injected into the electric grid. As can be observed, there is a 60 Hz component in i_{Fa}, and the grid current (i_{Sa}) is in counter phase to the grid voltage (v_{Sa}).

Figure 9.a shows the performance of the PV-SAF when the non-linear load demand is greater than the generated power. In this case, the load demands 422 W, while the PV generated power is 330 W. The load demand overbalance is supplied by the electric grid. It can be observed that i_{Sa} is sinusoidal and in phase with v_{Sa}. The load and PV-SAF currents on *d-q* axis are shown in Figures 9.b and 9.c. The average component of i_{Ld} (positive) is relative to the active power demand of the load and the average component of i_{Fd} (negative) is relative to the PV power generated and the losses in the converter. It can be seen that i_{Fq} compensates for i_{Lq} and the oscillating component of i_{Ld} is compensated for i_{Fd}.

The proposed PV-SAF is demonstrated to act by improving the power quality through the harmonic and reactive compensation of the load. At the same time, it injects into the electric grid the maximum power provided by the PV array.

C. Performance of PV-SAF Under Non-Linear Load in Night-Time Mode

In Night-time Mode, the PV array generated power is negligible; therefore, the PV-SAF acts only to compensate for harmonic and reactive components of the load, keeping V_{DC} at a fixed value. Figure 10 shows the performance of the PV-SAF in Night-time Mode when the load is non-linear, composed of a three-phase rectifier bridge with load *R-L* that demands 442 W. As shown in Figure 11.c, the Total Harmonic Distortion (THD) of i_{Sa} is 22.1% without the

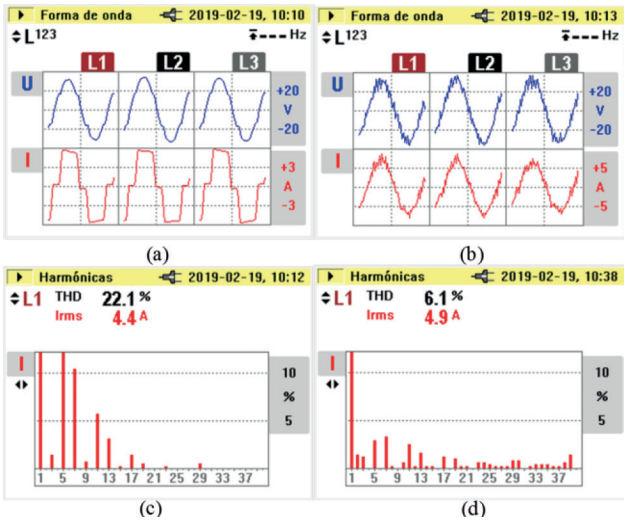

Fig. 11. Grid voltages and currents before (a) and after (b) the PV-SAF starts to act in the Night-time Mode obtained with the Minipa Power Quality Analyzer ET-5060C. The grid current THD before (c) and after (d) the switching start.

operation of PV-SAF. With the performance of PV-SAF, the THD is reduced to 6.1%, as shown in Figure 11.d, and is within the limits of harmonic distortion for current established by IEEE Std 519:1992 for $I_{SC}/I_L>20$ [7].

The THD analysis of the grid current in PV-SAF systems depends on the local load and PV generation. As the current ripples caused by the current controller are almost constant (in the HCC), when the PV generation is similar to the load demand, the fundamental component of the grid current is reduced, which causes an increase in DHT, but does not mean that the performance active filtering has been deteriorated.

Thus, the PV-SAF can compensate for the unwanted current components of non-linear loads even when there is no PV generation.

VI. CONCLUSION

In this paper, a control strategy for a single-stage PV-SAF system was proposed and validated experimentally by an experimental prototype. A GMPPT algorithm that estimates the possible location of power peaks was proposed and tested under several partial shading conditions, ensuring that the maximum power available from the PV array is extracted, unlike the conventional techniques used in previous proposals. The proposed GMPPT was performed at low tracking time and produced negligible voltage ripple. The experimental results showed that the GMPPT can be used in the PV-SAF system even with single-stage topology and in the occurrence of PSC. The elimination of current harmonics and reactive power was satisfactory, within the limits of IEEE Std. 519. PV-SAF has been demonstrated to be a modern and intelligent solution that integrates the distributed generation with improvement of the power quality.

ACKNOWLEGMENT

This work was partially supported by the Coordination for the Improvement of Higher Education Personnel (CAPES).

REFERENCES

[1] J. L. Sawin, J. Rutovitz, and F. Sverrisson, *Renewables 2018 Global Status Report*. Jun. 2018.

[2] P. R. M. Costa, M. R. de Castro, I. R. Machado, and V. P. Pinto, "A hybrid PI-LQG robust servo control method for STATCOM performance improvement," *Eletrônica de Potência*, vol. 25, no. 1, pp. 1–12, Mar. 2020.

[3] R. K. Varma, V. Khadkikar, and R. Seethapathy, "Nighttime application of PV solar farm as STATCOM to regulate grid voltage," *IEEE Trans. Energy Convers.*, vol. 24, no. 4, pp. 983–985, Dec. 2009.

[4] IEEE, "IEEE Standards for Interconnecting Distributed Resources with Electric Power System," *IEEE Std 1547-2003*, Jul. 2003.

[5] H. Markiewicz and A. Klajn, "Voltage Disturbances: Standard EN 50160," *Power Qual. Appl. Guid.*, 2004.

[6] E. Quitmann and E. Erdmann, "Power system needs – How grid codes should look ahead," *IET Renew. Power Gener.*, vol. 9, no. 1, pp. 3–9, Dec. 2014.

[7] IEEE Recommended Practices and Requirements for Harmonic Control in Electric Power Systems, "IEEE std 519-1992," *Ieee*, pp. 1–9, Apr. 1992.

[8] S. Ponnaluri, G. O. Linhofer, J. K. Steinke, and P. K. Steimer, "Comparison of single and two stage topologies for interface of BESS or fuel cell system using the ABB standard power electronics building blocks," in *2005 European Conference on Power Electronics and Applications*, pp.9, Jan. 2005.

[9] A. K. Barnes, J. C. Balda, and C. M. Stewart, "Selection of converter topologies for distributed energy resources," *Conf. Proc. - IEEE Appl. Power Electron. Conf. Expo. - APEC*, pp. 1418–1423, Feb. 2012.

[10] S. Silva, L. Sampaio, F. Oliveira, and F. Durand, "Pso-based Mppt Technique Applied To A Grid-tied Pv System With Active Power Line Conditioning Using A Feed-forward Dc-bus Control Loop," *Eletrônica de Potência*, vol. 21, no. 2, pp. 105–116, May 2016.

[11] T. Esram and P. L. Chapman, "Comparison of Photovoltaic Array Maximum Power Point Tracking Techniques," *IEEE Trans. Energy Convers.*, vol. 22, no. 2, pp. 439–449, Jun. 2007.

[12] M. Aureliano Gomes de Brito, L. Poltronieri Sampaio, G. de Azevedo e Melo, and C. Alberto Canesin, "Contribution For The Study Of The Main Pv Maximum Power Point Tracking Methods," *Eletrônica de Potência*, vol. 17, no. 3, pp. 592–600, Aug. 2012.

[13] S. A. Papathanassiou, P. S. Georgilakis, and E. I. Batzelis, "Energy models for photovoltaic systems under partial shading conditions: a comprehensive review," *IET Renew. Power Gener.*, vol. 9, no. 4, pp. 340–349, Nov. 2014.

[14] K. Chen, S. Tian, Y. Cheng, and L. Bai, "An Improved MPPT Controller for Photovoltaic System Under Partial Shading Condition," *IEEE Trans. Sustain. Energy*, vol. 5, no. 3, pp. 978–985, Jul. 2014.

[15] G.-J. Fang and K.-L. Lian, "A maximum power point tracking method based on multiple perturb-and-observe

method for overcoming solar partial shaded problems," in *2017 6th International Conference on Clean Electrical Power (ICCEP)*, Jun. 2017, pp. 68–73.

[16] M. A. Ghasemi, H. M. Foroushani, and M. Parniani, "Partial Shading Detection and Smooth Maximum Power Point Tracking of PV Arrays Under PSC," *IEEE Trans. Power Electron.*, vol. 31, no. 9, pp. 6281–6292, Sep. 2016.

[17] Q. Zhu, X. Zhang, S. Li, C. Liu, and H. Ni, "Research and Test of Power-Loop-Based Dynamic Multi-Peak MPPT Algorithm," *IEEE Trans. Ind. Electron.*, vol. 63, no. 12, pp. 7349–7359, Dec. 2016.

[18] A. Ramyar, H. Iman-Eini, and S. Farhangi, "Global Maximum Power Point Tracking Method for Photovoltaic Arrays Under Partial Shading Conditions," *IEEE Trans. Ind. Electron.*, vol. 64, no. 4, pp. 2855–2864, Apr. 2017.

[19] S. A. O. da Silva, L. P. Sampaio, F. M. de Oliveira, and F. R. Durand, "Feed-forward DC-bus control loop applied to a single-phase grid-connected PV system operating with PSO-based MPPT technique and active power-line conditioning," *IET Renew. Power Gener.*, vol. 11, no. 1, pp. 183–193, Jan. 2017.

[20] R. B. A. Koad, A. F. Zobaa, and A. El-Shahat, "A Novel MPPT Algorithm Based on Particle Swarm Optimization for Photovoltaic Systems," *IEEE Trans. Sustain. Energy*, vol. 8, no. 2, pp. 468–476, Apr. 2017.

[21] S. Rajendran and H. Srinivasan, "Simplified accelerated particle swarm optimisation algorithm for efficient maximum power point tracking in partially shaded photovoltaic systems," *IET Renew. Power Gener.*, vol. 10, no. 9, pp. 1340–1347, Oct. 2016.

[22] N. Kumar, I. Hussain, B. Singh, and B. K. Panigrahi, "Rapid MPPT for Uniformly and Partial Shaded PV System by Using JayaDE Algorithm in Highly Fluctuating Atmospheric Conditions," *IEEE Trans. Ind. Informatics*, vol. 13, no. 5, pp. 2406–2416, Oct. 2017.

[23] N. Pragallapati, T. Sen, and V. Agarwal, "Adaptive Velocity PSO for Global Maximum Power Control of a PV Array Under Nonuniform Irradiation Conditions," *IEEE J. Photovoltaics*, vol. 7, no. 2, pp. 624–639, Mar. 2017.

[24] N. Kumar, I. Hussain, B. Singh, and B. K. Panigrahi, "Peak power detection of PS solar PV panel by using WPSCO," *IET Renew. Power Gener.*, vol. 11, no. 4, pp. 480–489, Mar. 2017.

[25] S. Mohanty, B. Subudhi, and P. K. Ray, "A New MPPT Design Using Grey Wolf Optimization Technique for Photovoltaic System Under Partial Shading Conditions," *IEEE Trans. Sustain. Energy*, vol. 7, no. 1, pp. 181–188, Jan. 2016.

[26] J. P. Ram and N. Rajasekar, "A Novel Flower Pollination Based Global Maximum Power Point Method for Solar Maximum Power Point Tracking," *IEEE Trans. Power Electron.*, vol. 32, no. 11, pp. 8486–8499, Nov. 2017.

[27] D. F. Teshome, C. H. Lee, Y. W. Lin, and K. L. Lian, "A Modified Firefly Algorithm for Photovoltaic Maximum Power Point Tracking Control Under Partial Shading," *IEEE J. Emerg. Sel. Top. Power Electron.*, vol. 5, no. 2, pp. 661–671, Jun. 2017.

[28] K. Sundareswaran, S. Pedappati, and S. Palani, "MPPT of PV Systems Under Partial Shaded Conditions Through a Colony of Flashing Fireflies," *IEEE Trans. Energy Convers.*, vol. 29, no. 2, pp. 463–472, Jun. 2014.

[29] C. Manickam, G. P. Raman, G. R. Raman, S. I. Ganesan, and N. Chilakapati, "Fireworks Enriched P&O Algorithm for GMPPT and Detection of Partial Shading in PV Systems," *IEEE Trans. Power Electron.*, vol. 32, no. 6, pp. 4432–4443, Jun. 2017.

[30] S. Mohanty, B. Subudhi, and P. K. Ray, "A Grey Wolf-Assisted Perturb & Observe MPPT Algorithm for a PV System," *IEEE Trans. Energy Convers.*, vol. 32, no. 1, pp. 340–347, Mar. 2017.

[31] A. Chandra, B. Singh, K. Al-Haddad, S. Kumar, and I. Hussain, "An Adaptive Control Scheme of SPV System Integrated to AC Distribution System," *IEEE Trans. Ind. Appl.*, vol. 53, no. 6, pp. 5173–5181, Dec. 2017.

[32] N. Beniwal, I. Hussain, and B. Singh, "Second-order volterra-filter-based control of a solar PV-DSTATCOM system to achieve lyapunov's stability," *IEEE Trans. Ind. Appl.*, vol. 55, no. 1, pp. 670–679, Feb. 2019.

[33] S. Devassy and B. Singh, "Design and Performance Analysis of Three-Phase Solar PV Integrated UPQC," in *IEEE Transactions on Industry Applications*, Feb. 2018.

[34] R. K. Agarwal, I. Hussain, and B. Singh, "Three-phase single-stage grid tied solar PV ECS using PLL-less fast CTF control technique," *IET Power Electron.*, vol. 10, no. 2, pp. 178–188, Feb. 2017.

[35] S. Pradhan, I. Hussain, B. Singh, and B. Ketan Panigrahi, "Performance improvement of grid-integrated solar PV system using DNLMS control algorithm," *IEEE Trans. Ind. Appl.*, vol. 55, no. 1, pp. 78–91, Jan. 2019.

[36] V. Jain and B. Singh, "A Multiple Improved Notch Filter-Based Control for a Single-Stage PV System Tied to a Weak Grid," *IEEE Trans. Sustain. Energy*, vol. 10, no. 1, pp. 238–247, Jan. 2019.

[37] N. Beniwal, I. Hussain, and B. Singh, "Control and operation of a solar PV-battery-grid-tied system in fixed and variable power mode," *IET Gener. Transm. Distrib.*, vol. 12, no. 11, pp. 2633–2641, Jun. 2018.

[38] N. D. Tuyen and G. Fujita, "PV-Active Power Filter Combination Supplies," *IEEE Power Energy Technol. Syst. J.*, vol. 2, no. 1, pp. 32–42, Mar. 2015.

[39] H. Akagi, E. H. Watanabe, and M. Aredes, *Instantaneous Power Theory and Applications to Power Conditioning*. Sept. 2006.

[40] B. Yahia, D. Hind, and C. Rachid, "The Application of an Active Power Filter on a Photovoltaic Power Generation System," *Int. J. Renew. ENERGY Res. Djeghloud Hind al*, vol. 2, no. 4, Jan. 2012.

[41] N. Shah and C. Rajagopalan, "Experimental investigation of a multifunctional grid interactive photovoltaic system operating in partial shading conditions," *IET Renew. Power Gener.*, vol. 10, no. 9, pp. 1382–1392, Oct. 2016.

[42] S. Kumar and B. Singh, "A Multipurpose PV System

Integrated to a Three-Phase Distribution System Using an LWDF-Based Approach," *IEEE Trans. Power Electron.*, vol. 33, no. 1, pp. 739–748, Oct. 2018.
[43] F. J. Lin, K. H. Tan, Y. K. Lai, and W. C. Luo, "Intelligent PV Power System with Unbalanced Current Compensation Using CFNN-AMF," *IEEE Trans. Power Electron.*, vol. PP, no. c, p. 1, Sept. 2019.
[44] P. K. Ray, S. R. Das, and A. Mohanty, "Fuzzy Controller Designed PV based Custom Power Device for Power Quality Enhancement," *IEEE Trans. Energy Convers.*, vol. PP, no. c, p. 1, Nov. 2018.
[45] N. Kumar, B. Singh, B. K. Panigrahi, and L. Xu, "Leaky Least Logarithmic Absolute Difference Based Control Algorithm and Learning Based InC MPPT Technique for Grid Integrated PV System," *IEEE Trans. Ind. Electron.*, vol. 0046, no. c, Nov. 2019.
[46] N. Kumar, B. Singh, and B. K. Panigrahi, "LLMLF based Control Approach and LPO MPPT Technique for Improving Performance of a Multifunctional Three-Phase Two-Stage Grid Integrated PV System," *IEEE Trans. Sustain. Energy*, vol. PP, no. c, pp. 1–1, Jan. 2020.
[47] S. Buso, L. Malesani, and P. Mattavelli, "Comparison of current control techniques for active filter applications," *IEEE Trans. Ind. Electron.*, vol. 45, no. 5, pp. 722–729, Oct. 1998.
[48] B. K. Bose, "An adaptive hysteresis-band current control technique of a voltage-fed PWM inverter for machine drive system," *IEEE Trans. Ind. Electron.*, vol. 37, no. 5, pp. 402–408, Oct. 1990.
[49] M. Kale and E. Ozdemir, "An adaptive hysteresis band current controller for shunt active power filter," *Electr. Power Syst. Res.*, vol. 73, no. 2, pp. 113–119, Feb. 2005.
[50] N. Gupta, S. Singh, and S. Dubey, "DSP based adaptive hysteresis-band current controlled active filter for power quality conditioning under non-sinusoidal supply voltages," *Int. J. Eng. Sci. Technol.*, vol. 3, no. 4, pp. 236–252, Feb. 2011.
[51] L. Castañer and S. Silvestre, *Modelling Photovoltaic Systems Using PSpice®*. Wiley, Sept .2002.
[52] T. Markvart and L. Castañer, *Practical Handbook of Photovoltaics*. Elsevier, Oct. 2003.
[53] H. Patel and V. Agarwal, "Maximum power point tracking scheme for PV systems operating under partially shaded conditions," *IEEE Trans. Ind. Electron.*, Apr. 2008.
[54] J. Ahmed and Z. Salam, "An improved method to predict the position of maximum power point during partial shading for PV arrays," *IEEE Trans. Ind. Informatics*, vol. 11, no. 6, pp. 1378–1387, Dec. 2015.
[55] M. Rastogi, R. Naik, and N. Mohan, "A Comparative Evaluation of Harmonic Reduction Techniques in Three-Phase Utility Interface of Power Electronic Loads," *IEEE Trans. Ind. Appl.*, vol. 30, no. 5, pp. 1149–1155, Oct. 1994.
[56] M. Karimi-Ghartemani, H. Karimi, and M. R. Iravani, "A Magnitude/Phase-Locked Loop System Based on Estimation of Frequency and In-Phase/Quadrature-Phase Amplitudes," *IEEE Trans. Ind. Electron.*, vol. 51, no. 2, pp. 511–517, Apr. 2004.
[57] R. L. de A. Ribeiro, C. C. de Azevedo, and R. M. de Sousa, "A Robust Adaptive Control Strategy of Active Power Filters for Power-Factor Correction, Harmonic Compensation, and Balancing of Nonlinear Loads," *IEEE Trans. Power Electron.*, vol. 27, no. 2, pp. 718–730, Feb. 2012.

BIOGRAPHIES

Paulo Robson Melo Costa was born in Guaraciaba do Norte, CE, Brazil in 1994. He received the B.S. and M.S. degrees in electrical engineering from the Federal University of Ceará, Sobral, Brazil, in 2016 and 2019, respectively. He is currently a substitute professor at Federal University of Ceará. His areas of interest are power electronics, electricity conversion quality, electronic control systems and electrical machine actuation. Prof. Costa is member of the SOBRAEP.

Marcus Rogério de Castro was born in Fortaleza, Brazil. He received the B.S. and M.S. degrees in electrical engineering from the Federal University of Ceará, Fortaleza, Brazil, in 1999 and 2004, respectively, and the Ph.D. degree from the Université De Reims – Champagne Ardennes Reims, France, in 2010. Since 2011, he has been a Professor at the Federal University of Ceará, Sobral, Brazil. His research interests include static inverters, power factor correction circuits, dc-dc converters and their application to renewable energy systems.

Isaac Rocha Machado was born in Parnaíba, state of Piauí, Brazil. He received the B.Sc. and M.Sc. degrees in electrical engineering from the Federal University of Ceará (UFC), Fortaleza, Brazil, in 2004 and 2007, respectively, and the D.Sc. degree from the Federal University of Rio de Janeiro, Rio de Janeiro (COPPE/UFRJ), Brazil, in 2013. Since 2011, he has been a Professor at the Federal University of Ceará and the Post Graduate Program in Electrical and Computer Engineering (PPGEEC/UFC), in Sobral city, Brazil. He coordinates research and development studies in power electronics, working mainly on the following topics: energy processing, electrical drives, renewable energy sources (solar, wind and waves), active filters and FACTS. Prof. Isaac Machado is a member of the Brazilian Power Electronics Society (SOBRAEP) and the Institute of Electrical and Electronic Engineers (IEEE).

Edilson Mineiro Sá Jr. was born in Fortaleza, Brazil. He received the B.S. and M.S. degrees in electrical engineering from the Federal University of Ceará, Fortaleza, Brazil, in 1999 and 2004, respectively, and the Ph.D. degree from the Federal University of Santa Catarina, Florianopolis, Brazil, in 2010. Since 2008, he has been a Professor at the Federal Institute of Ceará, Sobral, Brazil, where he coordinates the Mechatronics Research Group (GPEM). His research interests include electronic ballasts, power factor correction circuits, dc–dc converters and their application to renewable energy systems, and LED drivers. Prof. Sá is member of the SOBRAEP.